Polyaniline/montmorillonite nanocomposites obtained by in situ intercalation and oxidative polymerization in cationic modified-clay (sodium, copper and iron)

A. Zehhaf [a], E. Morallon[b], A. Benyoucef [a*]

[a]*Laboratoire de Chimie Organique, Macromoléculaire et des Matériaux, Université de Mascara. Bp 763 Mascara 29000 (Algeria)*

[b]*Departamento de Química Física and Instituto Universitario de Materiales. Universidad de Alicante. Apartado 99. 03080 Alicante (Spain)*

[*]Corresponding author

e-mail: ghani29000@yahoo.fr

Telf.: +213-771707184

Fax: +213-45930118

Abstract

Polyaniline/montmorillonite nanocomposites (PANI/M) were obtained by intercalation of aniline monomer into montmorillonite (M) modified with different cations and subsequent oxidative polymerization of the aniline. The modified-clay was prepared by ion exchange of sodium, copper and iron cations in the clay (Na-M, Cu-M and Fe-M respectively). Infrared spectroscopy confirms the electrostatic interaction between the oxidized polyaniline (PANI) and the negatively charged surface of the clay. X-ray diffraction analysis provides structural information of the prepared materials. The nanocomposites were characterized by transmission electron microscopy and their thermal degradation was investigated by thermogravimetric analysis. The weight loss suggests that the PANI chains in the nanocomposites have higher thermal stability than pure PANI. The electrical conductivity of the nanocomposites increased between 12 and 24 times with respect to the pure M and this increase was dependent on the cation-modification. The electrochemical behavior of the polymers extracted from the nanocomposites was studied by cyclic voltammetry and a good electrochemical response was observed.

Keywords: Oxidative polymerization ; Polyaniline ; Nanocomposite ; Conducting polymer ; Montmorillonite ; Cation-Exchanged.

1. Introduction

During the last years, academic and industrial communities have dedicated intense efforts in the development of polymer/clay nanocomposite (PCN) materials. These materials usually demonstrate properties superior to conventional ones. In general, they combine both the characteristics of the inorganic template and the organic polymers at the molecular level [1]. Currently, the PCN material is found to be a promising system because the clay possesses a high aspect ratio and a platy morphology. It can be employed to boost the physical properties of bulk polymers being the mechanical properties a significant issue for application and development of these materials. Kim and White [2] reported a variety of organic modified montmorillonites to understand the contribution of the organophilicity of organoclay on the formation of the PCN [3-5].

The significance of the organoclay is that even less than 5 wt% of clay loading in any reinforcing component could improve hundreds of engineering properties which include fire retardancy [6-8], barrier resistance [9, 10], and ionic conductivity [11, 12]. It is clear from this evidence that PCNs are good demonstration of nanotechnology. Another interest in developing PCNs is that they can be applied immediately in commercial applications [13].

Polymer clay nanocomposites based on polyaniline/montmorillonite are obtained by the polymerization of anilinium ions within the interlayer space of montmorillonite (M) [14, 15].The electrically conducting polymers incorporated into clay have attracted great attention due to their potential technological applications in light-emitting diodes, lightweight battery electrodes, sensors, electro-optics, electromagnetic shielding materials, fuel cell electrodes and as anticorrosive coatings [16-18]. Among the conducting polymers, polyaniline (PANI) is a promising polymer due to its simple synthesis, high electrical conductivity and excellent chemical stability [19]. However, its poor thermal and mechanical properties restrict its

commercial applications and, therefore, methods to improve such properties are of great importance [20]. PANI/clay nanocomposites have numerous potential applications including electrodes for rechargeable batteries [21], electrodes for energy storage devices [22], electromagnetic interference shielding [23], electronic and optical devices [24], smart windows [22] and in light emitting diodes [22, 25].

Montmorillonite is constituted by two dimensional silicate anions with cations between the layers that can be easily exchanged. Thus, the interlayer spacing can be modified, depending on the cation intercalated. Therefore, the use of modified montmorillonite with different inorganic cations can affect properties like electrical conductivity of PCN. For this reason, in this work, the synthesis of nanocomposites of polyaniline with a natural montmorillonite modified with inorganic cations (Na^+, Cu^{2+} and Fe^{2+}) is reported. The polyaniline/clay nanocomposites were prepared by introducing the aniline monomer into the clay galleries containing Na^+, Cu^{2+}, Fe^{2+} (by cation exchange) and allowing to polymerize to form extended chains of PANI in the montmorillonite interlayers. The characterization of the PANI/clay nanocomposites by X-ray diffraction (XRD), transmission electron microscopy (TEM), Fourier transform Infrared spectroscopy (FTIR), thermogravimetric analysis (TGA) and cyclic voltammetry, is also performed.

2. Experimental

2.1. Materials

Aniline (ANI) (from Aldrich) was distilled under vacuum prior to use. Ammonium persulfate, perchloric acid, $CuSO_4$, NaCl and $FeSO_4$ were from Merck with p.a. quality and the water employed for the preparation of the solutions was obtained from an Elga Labwater Purelab Ultra system. A natural montmorillonite obtained from Tlemcen (Algeria) was used.

2.2. Preparation of metal ion-exchanged montmorillonites

10 g of natural montmorillonite (M) was suspended in 500 mL of doubly distilled water and stirred using a magnetic stirrer for 48 h. The suspension was centrifuged at 2000 rpm, and the clear supernatant was decanted. The resultant slurry was dispersed in 500 mL of water and the above procedure was repeated until the supernatant was free of any impurities. This procedure removed most of the organic impurities present in the clay along with some of the fine clay particles. The dry mass of the final clay was around 5 g. The slurry thus obtained was stirred for 24 h with either 100 mL of 1M NaCl (aq) or 1M $CuSO_4$ (aq) or 1M $FeSO_4$ (aq) solution to exchange cations present in the clay for Na^+, Cu^{2+} or Fe^{2+}. The resultant colloid was centrifuged and the supernatant discarded. The slurry thus obtained was then stirred with distilled water and, as before, the suspension was centrifuged and the supernatant was discarded. This procedure was repeated until the supernatant (tested using $AgNO_3$ (aq)) was free of Cl^- ions. The slurry thus obtained is the M containing hydrated Na^+ (Na-M), hydrated Cu^{2+} (Cu-M) or hydrated Fe^{2+} ions (Fe-M) within the interlayer spaces. The products were dried at 383 K, overnight and its composition was measured by X-ray fluorescence, obtaining the data in Table 1.

2.3. Preparation of PANI/montmorillonite nanocomposites

The nanocomposites were prepared by the intercalation of aniline in the modified montmorillonite (1g of Na-M, Cu-M or Fe-M), using an aniline solution and subsequent polymerization as described previously [26, 27]. Briefly, the modified-montmorillonite (Na-M, Cu-M or Fe-M) was dispersed in 100 mL of deionized water using ultrasonication for 5h. Then, 0.22 mol of aniline was added, followed by the addition of 1M perchloric acid $HClO_4$. The mixture was stirred for 24h until the monomer was intercalated into the montmorillonite.

Table 1. Elemental composition (wt%) of modified-montmorillonites (Na-M, Cu-M and Fe-M) and raw montmorillonite (M).

Composition (wt%)	SiO_2	Al_2O_3	Fe_2O_3	CaO	Na_2O	ZrO_2	MgO	K_2O	TiO_2	Cl^-	CuO
M	71.97	16.86	2.45	0.08	0.97	0.06	3.38	2.88	0.55	0.89	–
Na-M	73.40	17.72	1.95	0.01	2.66	0.01	2.60	1.48	0.17	–	–
Cu-M	74.45	16.35	2.06	0.01	–	0.01	1.80	1.63	0.35	–	3.34
Fe-M	72.81	17.35	5.43	0.01	–	0.01	2.75	1.48	0.16	–	–

Then, 0.1M ammonium persulfate solution (dissolved in 1M aqueous $HClO_4$) was added drop wise, and the mixture was stirred for 24 h at room temperature. The obtained precipitate of the nanocomposites was filtered, and washed several times with deionized water and methanol to remove unreacted monomers and $HClO_4$. The samples were dried under vacuum at 333 K for 24h.

2.4. Nanocomposites characterization

The X-ray diffraction of the powder nanocomposites were taken using a Bruker CCD-Apex equipment with a X-ray generator (Cu Kα and Ni filter) operated at 40kV and 40mA. X-ray fluorescence spectroscopy of the powder nanocomposites was made using a Philips PW1480 equipment with a UNIQUANT II software to determine elements in a semi quantitative way.

For recording the UV-Vis absorption spectra, a Hitachi U-3000 spectrophotometer was used. The solution of the polymer in N-methyl-2-pyrrolidone (NMP) was used for recording the spectrum. Fourier transform infrared (FT-IR) spectroscopy was recorded using a Bruker Alpha spectrometer. For TEM observations, the samples were dried under vacuum and supported on TEM grids. The images were collected using a JEOL (JEM-2010) microscope, working at an operation voltage of 200 kV.

2.5. Electrochemical characterization

The electrochemical behaviour of the polymers was studied by cyclic voltammetry after their extraction from the montmorillonite by dissolving in NMP. It is known that this kind of conducting polymers are soluble in NMP [28], while the clay remains in solid state. Thus, both components can be separated by filtration. The electrochemical measurements were carried out using a conventional three electrodes cell. The counter and reference electrodes were a platinum foil and a reversible hydrogen electrode (RHE), respectively. The polymer films were obtained by casting a drop of the NMP polymer solution over the working graphite electrode and heating with an infrared lamp to remove the solvent. The electrolyte used was 1M $HClO_4$ and all experiments were carried out at 50mV/s.

2.6. Electrical conductivity measurements

Electrical conductivity measurements were carried out using a Lucas Lab resistivity equipment with four probes in-line. The samples were dried in vacuum during 24 h and pellets of 0.013 m diameter were prepared using a FTIR mold by applying a pressure of 7.4 10^8 Pa.

3. Results and discussion

3.1. XRD characterization

The Na-M, Cu-M and Fe-M modified clays and the raw montmorillonite were characterized using X-ray diffraction to check changes in the interlayer spacing (Figure 1a). The XRD patterns show that the (001) diffraction peak between 5.5º and 6.5º, changes depending on the inorganic cation intercalated. Table 2 includes the d-spacing between the montmorillonite sheets calculated from the Bragg equation ($n\lambda = 2d\ sin\theta$, λ = 1.5418 Å Cu $K_{\alpha 1}$) [29], the ionic radii, the solvated radii (i.e., Stokes radii) and the maximum 2θ values of the peaks. This table shows that the size of the solvated cation rather than the ionic size determines the layer expansion [30].

The diffraction patterns of PANI/Na-M, PANI/Cu-M and PANI/Fe-M nanocomposites are shown in Figure 1b. Table 3 summarizes the XRD data obtained for the nanocomposites. Although the diffraction patterns are similar for PANI/Na-M and PANI/Fe-M samples, the (001) diffraction peak for PANI/Cu-M has a more pronounced peak at lower angles (2θ = 5.70º). PANI/Na-M nanocomposite has a basal spacing of 14.86 Å (which is higher than that for Na-M, Table 2) and this parameter is 15.48 Å for PANI/Cu-M sample which is also higher than the value obtained for Cu-M, suggesting the intercalation of PANI between the layers. The shoulder found in PANI/Cu-M at lower angles, suggests the existence of different conformations of the intercalated species. Yoshimoto et al. observed a similar change in the diffraction peak when they intercalated different amounts of anilinium salts into montmorillonite layers [31, 32]. These authors attributed this change to the existence of two types of conformations of intercalated species depending on the anilinium concentration [31]. Thus, in a similar way, the PANI/Cu-M sample can lead to different structures with different basal spacings.

The intercalation of Fe^{2+} and PANI into the M layers has been observed by XRD patterns. XRD pattern of Fe-M (Figure 1a) shows a shift in the peak position to lower 2θ

values (5.82º), which means that the basal spacing increases due to Fe^{2+} intercalation to 15.16 Å, what confirms the modification of the clay [33]. However, d-spacing value decreases after the intercalation of PANI into the Fe-M layers from 15.16 to 13.60 Å (Tables 2 and 3), what is due to the exfoliation of montmorillonite by the polymer.

Table 2. Ionic radii, Stokes radii, peak maximum and *d*-spacing of different inorganic cations intercalated in montmorillonite.

Ion	Ionic radii (Å)	Stokes radii (Å)	$2\theta_{max}$ Peak máximum	Basal spacing $d_{(001)}$ (Å)
Na^{+}	1.02	1.63	6.97	12.66
Cu^{2+}	0.73	5.79	6.42	13.75
Fe^{2+}	0.82	2.81	5.82	15.16

Table 3. Peak maximum and *d*-spacing of the PANI/clay nanocomposites.

Samples	PANI/Na-M	PANI/Cu-M	PANI/Fe-M
Peak maximum, 2θ max *(deg)*	5.94	5.70	6.49
Basal spacing, $d_{(001)}$ *(Å)*	14.86	15.48	13.60

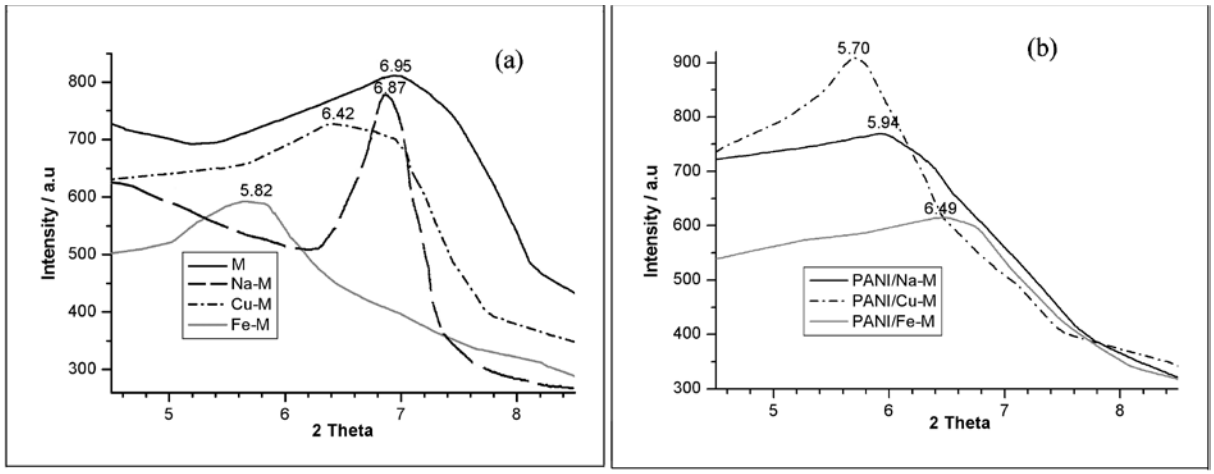

Figure 1. XRD diffraction patterns of (a) the montmorillonites (M, Na-M, Cu-M and Fe-M) ; (b) the nanocomposites (PANI/Na-M, PANI/Cu-M and PANI/Fe-M).

3.2. FT-IR Spectroscopy

The FTIR spectra of modified montmorillonites (Na-M, Cu-M, Fe-M) and PANI/clay nanocomposites (PANI/Na-M, PANI/Cu-M, PANI/Fe-M) are shown in Figure 2. The spectra of Na-M, Cu-M and Fe-M show the characteristic bands of silicate montmorillonite. These bands can be assigned as follows: the band at around 3623 cm^{-1} is due to O-H stretching vibration, the one at 1626 cm^{-1} is due to H-O-H bending, the one at 1007 cm^{-1} can be associated to Si-O stretching, the bands at 919 and 787 cm^{-1} are due to Al-O stretching and the one at 515 cm^{-1} is due to Si-O-Al stretching vibration [34].

The presence of PANI inside interlayer spaces of modified-montmorillonites results in the enhancement of the intensity of the 3200-3500 cm^{-1} band along with a decrease of intensity of the bands due to Si-O and Al-O vibrations. The increase in intensity of the 3200-3500 cm^{-1} band reflects the hydrogen bonding between the hydroxyl species and NH_3^+ group of the PANI. Likewise, the decrease in the intensity of the Si-O, Al-O, and Si-O-Al bands in presence of anilinium ions could be explained considering that when the protons in anilinium ions are hydrogen-bonded to the oxygen species of Si-O, Al-O, and Si-O-Al of the

montmorillonite, these bonds will weaken and the tetrahedral symmetry of these moieties in the clay will be distorted. This would result in the change of the IR band positions as well as in the decrease in the intensities of the bands.

The appearance of additional bands at around 1497 cm^{-1}, 1296 cm^{-1} and the shifts of the band positions are attributable to the amine group. The bands at 1586 and 1497 cm^{-1} have been assigned for benzenoid N-B-N and quinoid N=Q=N vibrations where B stands for benzenoid segments in polyaniline and Q for quinoid segments [35-37].

3.3. Electrical conductivity characterization

Table 4 shows the electrical conductivities of modified-montmorillonites. It can be observed an increase in the conductivity with the cation exchange, decreasing in the order Cu-M > Na-M > Fe-M. The presence of the polymer improves the electronic conductivity. The values of conductivity of the PANI/clay nanocomposites lie between 24.19 x 10^{-5} and 12.76 x 10^{-5} $S.cm^{-1}$ being the nanocomposite with copper the one that shows the higher conductivity.

The electrical conductivity of PANI/Fe-M was slightly increased with respect to PANI/Na-M sample. This may be attributed to the intercalation of the PANI chains between the Na-M layers which cause the formation of short conducting polymer chains. The contrary behavior was reported for the PANI/Fe-M that formed an exfoliated nanocomposite.

Table 4. The electrical conductivity values of modified montmorillonites and PANI/clay nanocomposites.

Samples	Na-M	Cu-M	Fe-M	PANI/Na-M	PANI/Cu-M	PANI/Fe-M
Conductivity (10^{-5} $S.cm^{-1}$)	1.74	4.51	0.96	12.76	24.19	15.45

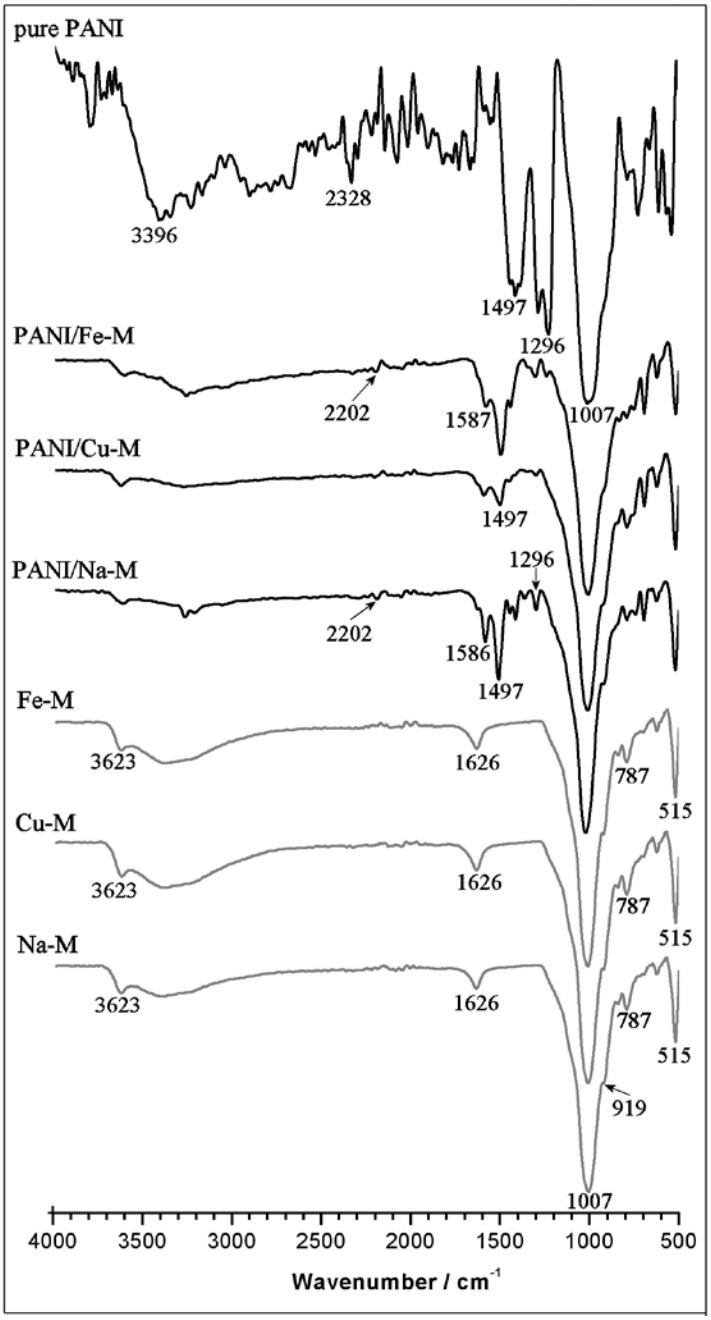

Figure 2. FTIR spectra of Na-M, Cu-M, Fe-M, PANI/Na-M, PANI/Cu-M, PANI/Fe-M and pure PANI.

3.4. UV-Vis spectroscopy

The UV-Vis spectra of nanocomposites in NMP solution are shown in Figure 3. The absorption maxima for the nanocomposites are included in Table 5. There are two absorption

bands in the electronic spectra of the samples. The first band at around ~350 nm is assigned to π-π^* transitions which corresponds to the band gap and the second band at above ~600 nm can be assigned to polaron-π^* exciton band or to a charge transfer band associated with the excitation of benzenoid to quinoid rings [38, 39].

3.5. Thermogravimetric analysis (TGA)

To analyze the thermal stability of the PANI/clay nanocomposites, thermogravimetric analysis was performed. Figure 4 shows the TGA curves for the Na-M, Cu-M and Fe-M, pure PANI and PANI/clay nanocomposites, measured under a nitrogen atmosphere. The degradation temperatures of the materials were measured from the intersection of the tangents of the initial part and the inflection point of the curve. The experiments for modified montmorillonites (Na-M, Cu-M and Fe-M) contain the typical features for M, a first process at low temperatures (at around 75ºC) which corresponds to the evolution of weakly bonded water molecules and a second one at around 600ºC that corresponds to the dehydroxilation of the octahedral sheet. The PANI/Na-M, PANI/Cu-M and PANI/Fe-M nanocomposites present two degradation stages. The first process occurs at around 100ºC that corresponds to the removal of adsorbed molecules such water and monomers that have not polymerized. The second degradation process occurs at around 250°C, with a weight loss between 10 and 20 wt% depending on the nanocomposite, that can be assigned to decomposition of the organic polymer [40]. Also, the weight loss for the second stage of decomposition was lower compared to pure PANI decomposition. The nanocomposites particles with a high aspect ratio may hinder the degradation process providing a barrier to preclude evaporation of small molecules generated during the thermal decomposition process. According to Zanetti et al. [41], the barrier effect of the clay increases during volatilization because of the reassembly of the silicate layers on the polymer surface by the thermal decomposition of the polymer

present in the nanocomposite. At higher temperatures a continuous weight loss is observed for all the nanocomposites.

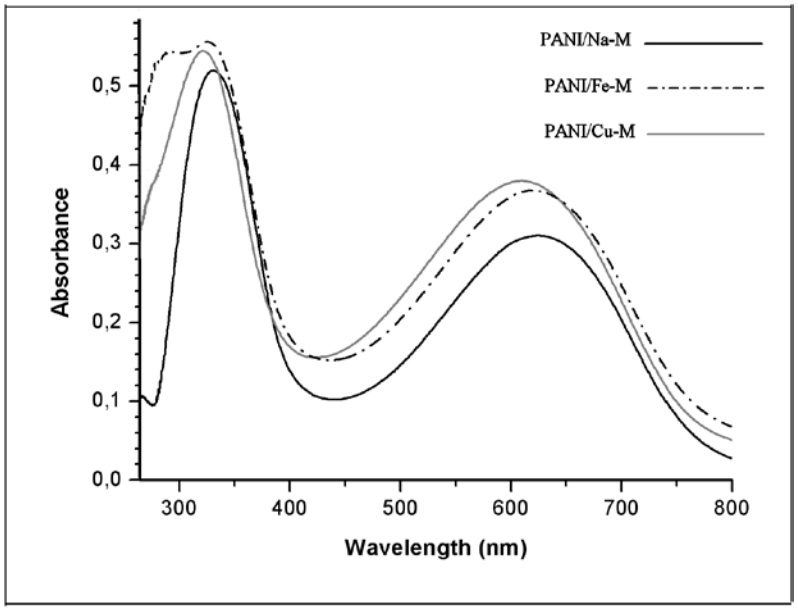

Figure 3. UV-vis spectra of the PANI/Na-M, PANI/Cu-M and PANI/Fe-M nanocomposites.

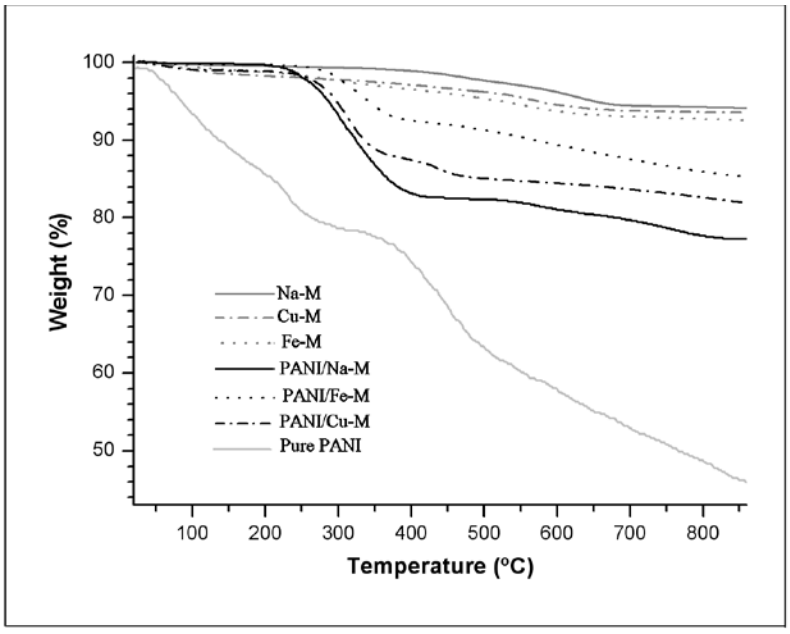

Figure 4. Thermogravimetric curves of Na-M, Cu-M, Fe-M, PANI/Na-M, PANI/Cu-M, PANI/Fe-M and pure PANI obtained in N_2 atmosphere at heating rate of 10°C/min.

Table 5. Position of the UV-Vis absorption bands of PANI/Na-M, PANI/Cu-M and PANI/Fe-M nanocomposites.

Nanocomposites	PANI/Na-M	PANI/Cu-M	PANI/Fe-M
Band gap (λ_{max} nm)	329	322	289-330
Exciton (λ_{max} nm)	625	611	622

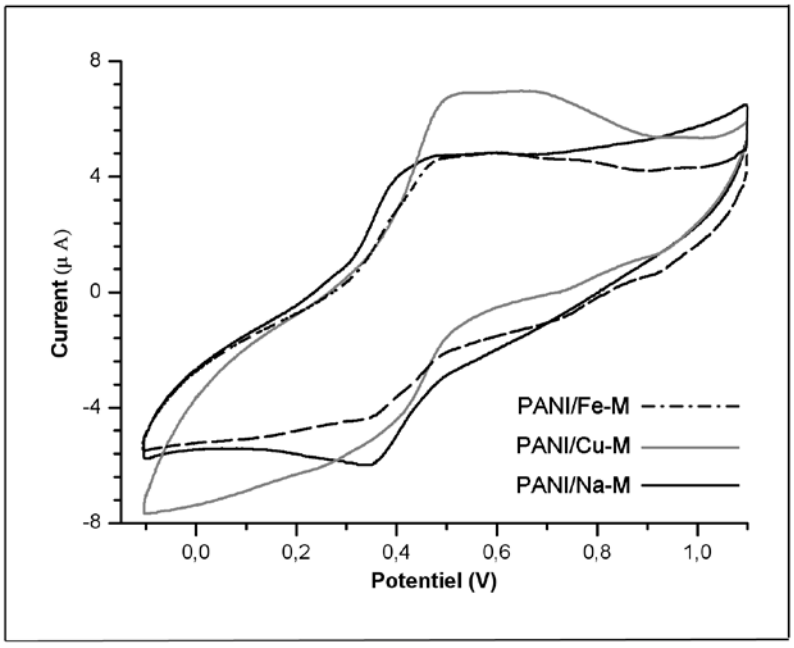

Figure 5. Cyclic voltammograms recorded for a graphite electrode covered by PANI/Na-M, PANI/Cu-M and PANI/Fe-M nanocomposites in 1M $HClO_4$ solution. Scan rate 50 mV/s.

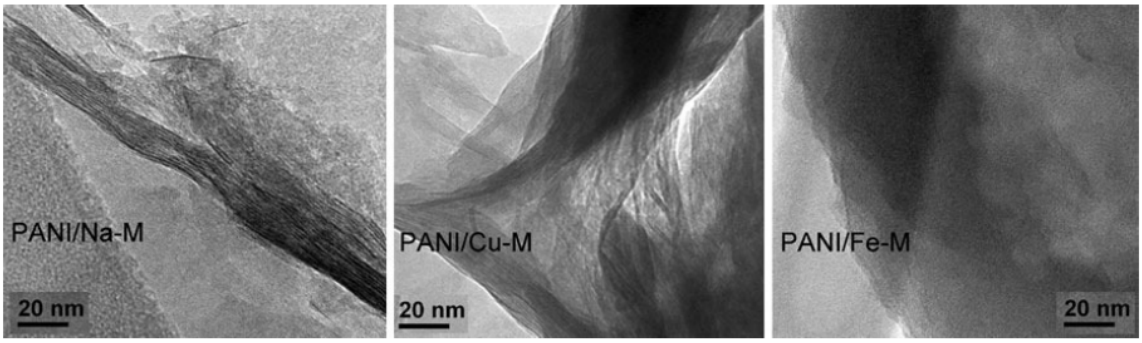

Figure 6. TEM images of the PANI/Na-M, PANI/Cu-M and PANI/Fe-M nanocomposites.

3.6. Electrochemical properties

Cyclic voltammetry experiments were performed to test the electroactivity of the PANI extracted from the nanocomposites. Figure 5 shows the steady voltammograms of PANI from PANI/Na-M, PANI/Cu-M and PANI/Fe-M samples, obtained in 1M $HClO_4$ solution at a scan rate of 50 $mV.s^{-1}$. In PANI from PANI/Cu-M nanocomposite, two overlapped redox processes are observed. The first one appears at 0.50/0.39 V, which results in a potential peak separation (ΔE_p) close to 110 mV; the second process is observed at 0.67/0.75 V and gives a ΔE_p value of 80 mV. The first redox process is due to the oxidation of the benzenoid form of polyaniline and the second one to the oxidation of the quinoid form of polyaniline. The voltammetric profiles for PANI from PANI/Na-M and PANI/Fe-M, show one redox process centered at 0.41/0.34V and 0.47/0.34V, respectively.

3.7. Transmission electron micrographs (TEM)

The TEM images of PANI/Na-M, PANI/Cu-M and PANI/Fe-M nanocomposites are shown in Figure 6. The images for PANI/Na-M and PANI/Cu-M samples show the clay layers in which polymer chains are intercalated. The PANI/Fe-M sample shows a mixed nanomorphology with the presence of some exfoliation of the clay.

4. Conclusions

A series of PANI/clay nanocomposites were prepared by the intercalation of aniline monomer into the interlayer space of montmorillonite modified with different inorganic cations (Na-M, Cu-M and Fe-M). FTIR spectroscopy evidences electrostatic interactions between the PANI chains and the clay layers. XRD and TEM observations suggest that PANI is intercalated into the layer of the clay for Cu-M and Na-M samples, and in the case of PANI/Fe-M, exfoliation of the clay is produced. Based on the TGA analysis, the PANI chains in the nanocomposites are more thermally stable than those of pure PANI. The room temperature electrical conductivity of the PANI/clay nanocomposites varies from 12.76×10^{-5} to 24.19×10^{-5} S/cm depending on the type of inorganic cation intercalated in the clay. Good electrochemical response was observed for the PANI grown into the montmorillonites (Na-M, Cu-M and Fe-M) in which the cyclic voltammograms show reversible redox processes.

Acknowledgements

This work was supported by the National Agency for the Development of University Research (ANDRU), the Directorate General of Scientific Research and Technological Development (DGRSDT) of Algeria. Ministerio de Economia y Competitividad and FEDER are also acknowledged (MAT2010-15273).

References

1. S.P. Liu, C.W. Liang, Int. J Heat Mass. Tran., **38**, 434 (2011).

2. Y. Kim, J.L. White, J. Appl. Polym. Sci. **96**, 1888 (2005).

3. J.J. Decker, S.N. Chvalun, S. Nazarenko, Polymer, **52**, 3943 (2011)

4. H. Akat, M.A. Tasdelen, F.D. Prez, Y. Yagci, Eur. Polym. J., **44**, 1949 (2008)

304 5. S. Kim, A.M. Palomino, Appl. Clay Sci., **51**, 491 (2011).

305 6. S. Qutubuddin, X. Fu, Y. Tajuddin, Polymer, **42**, 807-814 (2005).

306 7. G. Ragosta, G. Scarinzi, L. Mascia, Polymer, **45**, 2182 (2004).

307 8. J. Morawiee, A. Pawlak, M. Slouf, Eur. Polym. J. **41**, 1115 (2005).

308 9. K.M. Lee, C.D. Han, Polymer, **44**, 4573 (2003).

309 10. K.M. Lee, C.D. Han, Macromolecules, **36**, 804 (2003).

310 11. J.W. Gilman, Appl. Clay Sci. **15**, 31 (1999).

311 12. H.A. Klok, S. Lecommandoux, Adv. Mater. **13**, 1217 (2001).

312 13. C. Sanchez, G.J. Soler-Illia, A.A. de, F. Ribot, T. Lalot, C.R. Mayer, V. Cabuil, Chem.
313 Mater. **13,** 3061 (2001).

314 14. T. Changyu, C. Nanxi, Z. Qin, W. Ke, F. Qiang, Z. Xinyuan, Polym. Degrad. Stabil., **94**,
315 124 (2009).

316 15. L. Dongkyu, C. Kookheon, Polym. Degrad. Stabil., **75**, 555 (2002).

317 16. Y. Furukawa, F. Ueda, Y. Hyodo, I. Harada, T. Nakajima, T. Kawagoe, Macromolecules,
318 **21**, 1297 (1998).

319 17. K.G. Conroy, C.B. Breslin, Electrochim. Acta, **48**, 721 (2003).

320 18. J.E. Mark, Polymer data handbook. Oxford University, (1999).

321 19. G.M. Nascimento, V.R.L. Constantino, R. Landers, M.L.A. Temperini, Macromolecules,
322 **37**, 9373 (2004).

323 20. S. Yoshimoto, F. Ohashi, Y. Ohnishi, T. Nonami, Synthetic Met., **145**, 265 (2004).

324 21. M. Kaneko, H. Nakamura, J. Chem. Soc., Chem. Commun. **2**, 346 (1985).

325 22. D. Lee, K. Char, Polym. Degrad. Stabil. **75**, 555 (2002).

326 23. H Kuhn, R. Gregory, W. Kimbrell, Los Angeles, California, USA. **3**, 570 (1989).

327 24. H. Nishino, G. Yu, A.J. Heeger, T.A. Chen, R.D. Rieke, Synthetic Met., **68**, 243 (1995).

328 25. I.D. Parker, J. Appl. Phys. **75**, 1656 (1994).

329 26. K. Samrana, A. Shahzada, P. Jiri, P. Josef, M.J. Yogesh, J. Mat. Sci., **47**, 420 (2012).

330 27. Q. Wu, Z. Xue, Z. Qi, F. Wang, Polymer, **41**, 2029 (2000).

331 28. J.H. Sung, H.J. Choi, J. Macromol. Sci. B, **44**, 573 (2005).

332 29. D. Lee, S.H. Lee, K. Char, J. Kim, Macromol Rapid Comm., **21**, 1136 (2000).

333 30. F.C. Huang, F.J. Lee, C.K. Lee, H.P. Chao, Colloid Surface A, **239**, 41 (2004).

334 31. S. Yoshimoto, F. Ohashi, T. Kameyama, Macromol Rapid Comm., **25**, 1687 (2004).

335 32. I. Toumi, A. Benyoucef, A. Yahiaoui, C. Quijada, E. Morallon, J. Alloy Compd., **551**, 212
336 (2013)

337 33. D. Lee, K. Char, S.W. Lee, Y.W. Park, J. Mater. Chem., **13**, 2942 (2003).

338 34. R.E. Grim, McGraw-Hill International Series, Sydney, Australia. 261 (1968).

339 35. R. Murugeshan, E. Subramanian, Mater. Chem. Phys., **77**, 860 (2002).

340 36. S. Sharma, C. Nirkhe, S. Pethkar, A.A. Aathaawale, Sensor. Actuat. B-Chem., **85**, 131
341 (2002).

342 37. M.J. Wilson, Infrared Methods, Chapman and Hall, London. (1994).

343 38. K. Samrana, A. Shahzada, P. Jiri, P. Josef, M.J. Yogesh, J. Mater. Sci., **47**, 420 (2012).

344 39. O. Yang, Y. Zhang, H. Li, Y. Zhang, M. Liu, J. Luo, L. Tan, H. Tang, S. Yao, Talanta, **81**,
345 664 (2010).

346 40. M.A. Soto-Oviedo, O.A. Araujo, R. Faez, M.C. Rezende, M.A. DePaoli, Synthetic Met.,
347 **156**, 1249 (2006).

348 41. M. Zanetti, T. Kashiwagi, L. Falqui, G. Camino, Chem. Mater., **14**, 881 (2002).